Computer-guided Binding Mode Identification and Affinity Improvement of an LRR Protein Binder without Structure Determination

Yoonjoo Choi[1,†], Sukyo Jeong[1,†], Jung-Min Choi[1], Christian Ndong[2], Chris Bailey-Kellogg[3], Karl E. Griswold[2,4,5], and Hak-Sung Kim[1,*]

[1]Department of Biological Sciences, Korea Advanced Institute of Science and Technology, Daejeon, 34141, Korea.

[2]Thayer School of Engineering, Dartmouth College, Hanover, NH 03755, USA.

[3]Department of Computer Science, Dartmouth College, Hanover, NH 03755, USA.

[4]Norris Cotton Cancer Center at Dartmouth, Lebanon, NH 03766, USA.

[5]Department of Biological Sciences, Dartmouth College, Hanover, NH 03755, USA.

† These authors contributed equally

Correspondence

Hak-Sung Kim

Department of Biological Sciences, Korea Advanced Institute of Science and Technology, Daejeon, 34141, Korea.

Tel: +82-42-350-2616

Email: hskim76@kaist.ac.kr

Keywords

Protein binding mode; Computational protein design; LRR protein; Epitope mapping; Binding affinity

Abstract

Precise binding mode identification and subsequent affinity improvement without structure determination remain a challenge in the development of therapeutic proteins. However, relevant experimental techniques are generally quite costly, and purely computational methods have been unreliable. Here, we show that integrated computational and experimental epitope localization followed by full-atom energy minimization can yield an accurate complex model structure which ultimately enables effective affinity improvement and redesign of binding specificity. As proof-of-concept, we used a leucine-rich repeat (LRR) protein binder, called a repebody (Rb), that specifically recognizes human IgG_1 ($hIgG_1$). We performed computationally-guided identification of the Rb:$hIgG_1$ binding mode and leveraged the resulting model to reengineer the Rb so as to significantly increase its binding affinity for $hIgG_1$ as well as redesign its specificity toward multiple IgGs from other species. Experimental structure determination verified that our Rb:$hIgG_1$ model closely matched the co-crystal structure. Using a benchmark of other LRR protein complexes, we further demonstrated that the present approach may be broadly applicable to proteins undergoing relatively small conformational changes upon target binding.

Author Summary

It is quite challenging for computational methods to determine how proteins interact and to design mutations to alter their binding affinity and specificity. Despite recent advances in computational methods, however, *in silico* evaluation of binding energies has proven to be extremely difficult. We show that, in the case of protein-protein interactions where only small structural changes occur upon target binding, an integrated computational and experimental approach can identify a binding mode and drive reengineering efforts to improve binding affinity or specificity. Using as a model system a leucine-rich repeat (LRR) protein binder that recognizes human IgG_1, our approach yielded a model of the protein complex that was very similar to the subsequently experimentally determined co-crystal structure, and enabled design of variants with significantly improved IgG_1 binding affinity and with the ability to recognize IgG_1 from other species.

Introduction

In the development of therapeutic proteins and vaccines, the efficacy and effectiveness are largely determined by their binding modes and affinities [1-6]. Binding mode identification and affinity improvement have generally relied on labor-intensive and time-consuming experimental approaches [7], such as determination of complex structures by X-ray crystallography, and generation and screening of large libraries. To overcome these bottlenecks, considerable effort has been made to develop alternative computational methods [8, 9]. Despite some notable advances, however, computational determination of binding mode and *in silico* improvement of binding affinity remain challenging in general, and purely computational approaches have been insufficiently reliable for such purposes [10-13] and association energies [14-17]. Recent rounds of the Critical Assessment of Predicted Interactions (CAPRI) have also shown that current computational methods are not successful in identifying the actual binding mode [18]. Thus, the problem of predicting protein-protein interations is often regarded as a "Holy Grail" in the computer-aided protein engineering [14].

Leucine-rich repeat (LRR) proteins have a rigid horseshoe-like structural feature and play key roles in many biological processes [19], including the immune system [20-23] and cellular processes [24-26]. LRR proteins constitute one of the most common protein families found in a wide range of species, and more than 2,000 LRR proteins have been identified [27, 28]. Typical examples include toll-like receptors (TLR) of the mammalian innate immune system [21], and variable lymphocyte receptors (VLR) of the jawless vertebrate adaptive immune system [23]. Considering the importance and abundance of LRR proteins in nature, a broadly enabling strategy for modeling and controlling LRR binding can help in understanding of their functions as well as leveraging their recognition abilities for therapeutic applications.

80 We previously developed a computationally-driven epitope localization method, EpiScope,
81 through which a target antibody's binding is evaluated against a small, optimized panel of
82 antigenic variants to test hypothesized epitope locations [11]. EpiScope was shown to successfully
83 predict a general epitope region, but not providing detailed information about binding mode. Here,
84 as the extension of EpiScope, we demonstrate an integrated computational and experimental
85 approach to identifying the binding mode that further enables affinity improvement and redesign
86 of binding specificity. As proof-of-concept, we employed an LRR protein binder that specifically
87 recognizes an immunoglobulin G (IgG), for which the binding mode was completely unknown.
88 This work represents a challenging model system for affinity improvement and redesign of
89 specificity due to high structural conservation combined with sequence diversity across species.
90 We show that our approach effectively narrowed down the location of the binding interface, and
91 the full-atom energy minimization identified a native-like complex model closely matching a
92 experimentally determined X-ray crystal structure. Further computational analyses of the
93 identified model complex allowed the design of LRR protein binders with significantly increased
94 affinity and altered binding specificity.

95

96 ## Results

97 **Binding mode identification of an LRR protein binder**

98 In an effort to exploit the structural and functional features of LRR proteins for biotechnological
99 and medical applications, we previously developed an LRR protein binder, called a "repebody
100 (Rb)" [29]. Here, a human IgG_1 ($hIgG_1$)-binding repebody, named RbF4 [30], was targeted for
101 computationally-driven binding mode identification and subsequent affinity improvement as well
102 as redesign of binding specificity. There is indirect evidence that RbF4 recognizes the constant

103 region of $hIgG_1$ (hFc) [30, 31], but the actual epitope residues and the binding mode were
104 unknown. RbF4 has a typical LRR protein sequence motif, whose structural scaffold consists of
105 three major parts: an N terminal cap (LRRNT), LRR modules (LRRVs), and a C terminal cap
106 (LRRCT) with an additional loop (**Fig. S1**). In contrast to the complementarity determining regions
107 of antibodies, the target-binding sites of a repebody (the LRRVs) comprise parallel beta strands
108 which are assumed to remain unchanged upon target binding. During the development of RbF4,
109 three variable residues on each of modules LRRV2, LRRV3, and LRRV5 were randomized and
110 subjected to a phage display selection [30].

111 To identify the binding mode of RbF4-hFc, we first localized the RbF4 epitope on hFc
112 using EpiScope. This computational method first predicts mutations which appear to both disrupt
113 a target binding according to the models and maintain antigen stability; it then optimizes targeted
114 sets of antigenic variants that combine these mutations so as to efficiently confirm and reject the
115 various epitope hypotheses [11]. For antibody-antigen pairs, an average of three variants, each
116 with three mutations designed to disrupt binding and maintain stability, were shown to be sufficient
117 to test all of the docking models over a benchmark set of targets, in each case yielding at least one
118 variant expected to include the true epitope region. It should be noted that this form of epitope
119 localization indicates the general region where the protein is likely to bind, but does not provide a
120 binding mode in detail.

121 In this study, the ClusPro webserver was employed to dock the RbF4-hFc pair as previously
122 [11]. We used a crystal structure of the unbound form of hFc (PDB code: 3AVE) and a homology
123 model of RbF4 for the docking (**Table 1**), assigning attractions at the residues of the binding site
124 (LRRV modules from 2 to 5) in order to focus docking to this region. The affinity improvement
125 of repebodies is similar to that of antibodies, in that diversity is generated in the binding region of

126 the repebody/antibody followed by selection of variants with improved affinity. This leads to an
127 assymetric representation of amino acids, and thus we used the antibody docking mode and its
128 associated assymetric scoring (Antibody Mode). As a result, a total of 29 target-bound complex
129 models were generated (**Table 1**).

130 We note that each mutation is duplicated due to the dimeric nature of Fc. The selected
131 variants include Var 1 (Q362E/N389E/N390K), Var 2 (H268K/E269K/R292L), and Var 3
132 (H310A/N315K/H435K). The binding affinities of RbF4 against the variants were experimentally
133 evaluated by isothermal titration calorimetry (ITC), and binding of Var 3 was shown to be
134 disrupted approximately 3-fold compared to wild-type hFc, with a decrease in K_d from 128 nM to
135 427 nM (**Fig. 1B** and **Fig. S2**). This result confirms that RbF4 indeed binds to hFc. Since, as
136 previously observed [11], it is likely that not all positions mutated in a variant are equally important
137 for binding, we also measured the binding affinities of the single mutations comprising Var 3. Two
138 of the single mutations (H310A and N315K) led to meaningful two-fold reductions in binding
139 affinity (194 and 187 nM, respectively), whereas the binding affinity of H435K remained similar
140 to (or even a little stronger than) that of wild-type hFc. From these results, we conclude that RbF4
141 likely contacts H310 and N315, but not H435.

142 Seven RbF4-hFc docking models were consistent with the binding results; RbF4 makes
143 contacts with H310 and N315, but not H435 or the six other positions mutated in Vars 1 and 2
144 (**Fig. 1C**). We hypothesized that the all-atom force field energy could largely capture the binding
145 free energy landscape. The seven docking models were ranked by total energy according to the
146 AMBER99sb force field [33] after full-atom minimization using the Tinker molecular dynamics
147 package [34]. We determined the complex structure by X-ray crystallography (deposited as PDB
148 ID: 6KA7), and comparison of the crystal structure with the docking models confirms that the

149 binding mode of the docking model with the lowest energy (**Fig. 1C** and **D**, blue model) and that
150 of the crystal structure are indeed extremely similar (f_{nat}: 0.43 and I-RMSD: 2.89 Å, see **Fig. 2** and
151 **Table S2**). The full atom structure minimization changed the overall Fc structure, and
152 consequently one complex model had a slightly better I-RMSD than the lowest-energy model, but
153 the lowest-energy model better maintained interactions across the interface and thus had a much
154 better f_{nat} (**Fig. S3A**). These results demonstrate the utility of our integrated computational and
155 experimental approach to identifying a native-like complex model for an LRR protein: first a
156 computational method designs sets of mutational variants to probe docking models; then
157 experimental binding assays effectively filter the docking model candidates; finally full-atom
158 minimization ranks the filtered docking models. It is noteworthy that epitope localization is an
159 essential step for precise binding mode identification, and ranking docking models using the force
160 field energy alone may be insufficient for finding a native-like model (**Fig. 2B** and **C**). Furthermore,
161 testing the individual mutations comprising a selected variant was important in this case; if all of
162 the three positions in Var 3 were assumed to be important, there would be only two possible
163 docking models (**Fig. S3B**), and while the interface region of the lower energy model is largely
164 correct, its binding orientation is completely reversed.

165

166 **Redesign of binding specificity based on the modeled complex**

167 Based on the model complex structure, we redesigned RbF4 to alter its binding specificity. RbF4
168 was previously determined to be highly specific for human IgG_1, showing weak and negligible
169 cross-reactivities against mouse IgG_1 and rabbit IgG [30, 31]. The confirmed complex model here
170 reveals that the loop (**Fig. S1**) may be largely responsible for the binding specificity of RbF4
171 toward hFc (**Fig. 1D**). To obtain further insight into this possible source of specificity, we

172 investigated the Fc sequences of IgGs from three species: human (hFc), mouse (mFc), and rabbit
173 (rFc). The modeled RbF4:hFc complex shows that the RbF4 loop forms a tight contact with the
174 positions where amino acids differ among hFc, mFc, and rFc (**Fig. 1D**), strongly supporting a
175 crucial role for this loop in the observed binding specificity of RbF4. We thus reasoned that
176 engineering the loop could yield a variant of RbF4 showing cross-reactivities for Fc from other
177 species. To prove our hypothesis, we replaced the loop sequence of RbF4 starting at position 239,
178 RNSAGSVA, with the truncated but flexible amino acid pair GG. We measured with ITC assays
179 the binding affinities of the resulting loop-truncated RbF4 variant (RbF4-LT) against the IgGs
180 from the three species: $hIgG_1$ (Trastuzumab), mouse IgG_1 ($mIgG_1$), and rabbit IgG (rIgG).

181 As shown in our previous work [31], the original RbF4 binds strongly to $hIgG_1$ with a
182 binding affinity of 128.7 nM, whereas binding weakly to $mIgG_1$ with an 8-fold lower affinity of 1
183 μM, and has a negligible binding affinity for rIgG (**Fig. 3** and **Fig. S4**). The loop-truncated variant
184 (RbF4-LT) displayed improved binding affinity for rIgG (1.2 μM), indicating that the loop is
185 indeed involved in the binding specificity of RbF4 for $hIgG_1$. Its binding affinity for $mIgG_1$ was
186 also improved (775 nM), whereas that for $hIgG_1$ decreased to a level similar to that for $mIgG_1$ (598
187 nM). It bears noting that the variant was designed based only on the modeled binding mode, prior
188 to the determination of the X-ray co-crystal structure. The results thus demonstrate that our
189 integrated approach can provide sufficiently accurate complex models for the redesign of binding
190 specificity.

191

192 **Improvement of binding affinity based on the modeled complex**

193 Our final goal is to use computational design to improve the binding affinity of RbF4 against
194 different IgGs. As we saw in determining the best complex model, while the full-atom force field

195 energy alone did not identify the near-native complex, it did largely capture the binding energy
196 landscape. We thus again used the AMBER99sb total energy to select loop mutations predicted to
197 simultaneously improve binding affinities of RbF4 against multiple targets. To reduce the search
198 space, FoldX [35] was employed to fast-scan possible mutations in the loop (**Fig. S5**), since we
199 observed that FoldX is particularly accurate in predicting disruptive mutations (PPV > 0.9 for
200 antibody-antigen pairs) [36]. The predicted binding energy values at G243 indicate that the
201 inclusion of the loop may not enhance a binding affinity for rIgG. Thus we aimed to design an
202 RbF4 variant which can bind to both $hIgG_1$ and $mIgG_1$ with high binding affinities. The FoldX
203 scan suggests that S241M may substantially enhance the binding affinities for $hIgG_1$ and $mIgG_1$.
204 The mutation was also observed during the phage display affinity maturation for the $mIgG_1$-
205 specific repebody [31]. We then fixed S241M and introduced all other amino acids *in silico* at
206 S244. The AMBER99sb force field energy was used to minimize the variants. The binding energy
207 prediction indicated that S241M with S244R (RbF4-MR) may significantly improve the binding
208 affinities for both IgGs (**Fig. S6**). We tested this variant, and the ITC binding assay indeed showed
209 that RbF4-MR strongly binds to the two IgGs as predicted, and the binding affinity for $mIgG_1$ was
210 markedly increased (1 μM to 168.1 nM, **Fig. 3**).

211

212 **General applicability of the binding mode identification method**

213 To assess the general applicability of our integrated approach to identifying a binding mode, we
214 investigated three known Rb targets whose co-crystal structures are available (**Table 1**):
215 Interleukin-6 (IL-6: 4J4L) [29], epidermal growth factor receptor (EGFR: 4UIP) [37] and
216 complement component 5a (C5a: 5B4P) [38]. We first investigated the importance of using
217 ClusPro's "antibody mode" for Rb docking. Docking without the antibody mode option resulted

218 in a larger number of docking models, but the overall accuracy of the docking models proved to
219 be worse than that of those generated with the option enabled (**Table 1**). The antibody mode puts
220 a lower weight on the DARS [39] energy term than other docking modes [32]. In order to improve
221 binding affinities of antibodies and other protein binders, mutations are extensively made on only
222 one of the interacting partners (e.g., complementarity determining regions in antibodies) [40]. Thus,
223 the statistics of observed amino acid frequencies for the binding interface regions are different.
224 DARS assumes a symmetry interaction, which is beneficial for general protein-protein docking,
225 whereas it is worse for antibody-antigen pairs [40]. We likewise hypothesize that interaction
226 assymetry, captured in ClusPro's antibody mode, leads to improved prediction accuracy for
227 repebody binding and other affinity matured protein binders.

228 Consistent with the results above for RbF4-hFc, only a small number of variants were
229 sufficient to localize the epitopes (two for C5a and EGFR, and four for IL-6). The filtering process
230 resulted in a small set of docking models including native-like ones (5 to 12 models; solid circles
231 in **Fig. 4**). In order to identify the most native-like docking model, the ClusPro score was initially
232 considered to rank the filtered docking models, but it was observed to be unreliable (**Fig. S7**). In
233 constrast, but consistent with the RbF4-hFc results, **Figure 4** shows that ranking based on the
234 AMBER99sb force field energy successfully discriminated high-quality docking models for IL-6
235 and EGFR. It bears noting that the prior epitope localization was again critical; ranking by the
236 force field energy alone was not sufficient to find native-like docking models. For example, in the
237 case of IL-6, there are two incorrect docking models with lower energies than the most native-like
238 model, but both of them are not in contact with true epitope residues and thus were filtered out.

239 The C5a case provides an additional insight into precise binding mode prediction (**Fig. 4**,
240 bottom row). While the binding interfaces were mostly correct (15 out of 18 correct interface

241 residues: 83%), the predicted binding mode was completely inverted (N terminal to C, and vice
242 versa). During the affinity improvement of the C5a-specific Rb, it was observed that some LRRV
243 modules gave rise to a negligible increase in the binding affinity [38], suggesting that only LRRV1
244 and 2 were responsible for interacting with C5a. We thus hypothesized that the accuracy of
245 structural modeling and an incorporation of the paratope information may also enhance docking
246 quality. The four possible combinations of hypotheses (incorporation of the phage display
247 information versus no incorporation, and a homology-model target versus a crystal structure target)
248 revealed that the use of a high-quality structure (here the crystal structure) was not sufficient for
249 accurate binding mode identification (**Fig. 5**). No paratope information with the crystal structure
250 resulted in worse correlations than the model with precisely annotated paratopes (Spearman ρ for
251 f_{nat} and I-RMSD of crystal structures: -0.1 and 0.1, and those of models with precise paratope
252 definition: -0.7 and 0.19, respectively). The ideal case (crystal structures with precise paratopes)
253 led to extremely accurate results (I-RMSD: 0.62Å and f_{nat}: 0.76) with high correlations to the
254 crystal structure (Spearman ρ for f_{nat} and I-RMSD: -0.79 and 0.71).

255 This retrospective study demonstrated critical criteria for accurate binding mode
256 identification. The full-atom force field energy can effectively discriminate the most native-like
257 docking model when combined with an initial epitope localization using experimental data to filter
258 the models; on its own it may not be sufficient. As also observed in the previous study with
259 antibodies [11], high-quality antigen structures are not required for epitope localization; homology
260 models generally suffice. However, they are necessary to generate and predict native-like binding
261 modes. Finally, while, like antibodies, repebodies have well-defined target-binding sites, not all of
262 them are actually involved in target binding. The inclusion of paratope information (e.g., residues

263 contributing to phage display selection) was shown to improve the quality of docking models and
264 binding mode prediction.

265

266 **Discussion**

267 Precise binding mode identification of protein binders is crucial for the development of therapeutic
268 proteins, but they have heavily relied on labor-intensive experimental approaches. Computational
269 methods that do not require structure determination offer a way to accelerate development
270 processes and understanding of mechanisms of action, advancing the potential utility of relevant
271 proteins in translational and basic research. We chose LRR proteins as a model system to evaluate
272 the utility of an intergrated computational and experimental approach to identifying binding modes
273 and reengineering binding affinity and specificity, since theses proteins not only represent a
274 promising therapeutic scaffold, but they also have the important advantage of undergoing small
275 structural changes upon target binding. We extensively studied one LRR protein binder targeting
276 the constant domain of human IgG_1 (hFc). Computaional and experimental epitope localization
277 followed by full-atom energy minimization with the AMBER99sb force field enabled the
278 successful selection of a docking model which was confirmed to be most native-like according to
279 the independently solved X-ray crystal structure. The further utility and potential of our
280 computationally-guided binding mode identification were demonstrated by successfully
281 implementing the resulting model to design variants with increased binding affinity and altered
282 specificity.

283 Unlike epitope localization or binding site identification, which do not require extremely
284 native-like binding modes in the sampling step [11], the inclusion of native-like complex models

285 is absolutely necessary for further affinity improvement from models. In general, the sampling
286 quality of antibody-antigen docking often depends on the targets; however, in our case, native-like
287 models were nearly always included among the samples, likely due to the rigid nature of LRR
288 domains. Therefore, we anticipate that this approach may in principle be applicable not only to
289 LRR domains, but also to any other proteins with rigid binding sites. As also demonstrated by the
290 success of interface-guided docking methods [41-43], the exact definition of binding interfaces
291 including paratope mutational data from phage display selection is also important.

292 As repeatedly shown here, selection of a docking model based only on the molecular
293 modeling energy may be misleading, perhaps due to the inaccuracy of the energy functions [44].
294 Mutagenesis-based verification and filtering of docking models generally focused on the correct
295 epitope region, and they were shown to be necessary here in order to complement imperfect energy
296 scores. The epitope localization method used in this study, EpiScope [11], provided an optimal set
297 of mutational variants; here requiring only six sets of *in vitro* experiments to effectively localize
298 the epitope. With the epitope thereby localized, full-atom minimization enabled ranking of filtered
299 docking models, resulting in identification of a native-like docking model.

300 The successful modeling of binding mode directly enabled the design of binding
301 specificities and affinities. From the model, we were able to identify key contributors to the binding
302 specificity of RbF4 for the IgGs and engineer a simple manipulation to entirely change its binding
303 specificity. Furthermore, since the force field energy is indicative of binding energy, we were able
304 to select mutations based on the energy and dramatically improve binding affinities as predicted.
305 However, as discussed above, this holds only with a good model of binding, as otherwise design
306 only based on the energy may result in wrong predictions. For example, the force field energy
307 prediction suggeests that RbF4-MR would also have a good binding affinity to $hIgG_1$ though the

actual binding affinity was not improved (**Fig. S7**). ~~From the two studies of the binding mode prediction and affinity improvement, the force field energy prediction becomes informative only if actual binding is known, i.e. supportive data from experiments are critical in practice.~~

Methods

Computational Methods

To design mutations for epitope localization, we used EpiScope with default settings [11]. three mutations per binding patch, and one pareto-optimal curve and two suboptimal ones. The docking models were generated using the ClusPro webserver [32], initially using "Antibody mode" [40], and later a separate set was generated without that option. The non-CDR masking option was disabled, but the binding sites were masked for attraction and the convex side for repulsion (**Fig. S1A**). As with the models of the targets, the complex models were minimized using the Tinker molecular dynamics package [34] with the AMBER99sb parameter set [33] and the GB/SA implicit solvent model [45]. The total energy was used to rank complex models, and FoldX (ver. 4) was employed to fast filter binding disruptive mutations [35]. A complex structure is repaired and optimized using 'RepairPDB'. Given a mutation or set of mutations, the effect on binding is then calculated using the 'BuildModel' command.

There are currently three Rb-target complex structures in the PDB: binders to IL-6 (PDB code 4J4L), EGFR (4UIP), and C5a (5B4P). Unbound forms of the target structures were used for docking (**Table 1**). There is a missing loop in the structure of IL-6 (1ALU chain A: 52 SSKEALAEN). The loop was filled using MODELLER [46] and all the backbone atoms of the loop were minimized using Tinker as described above. While repebodies have a very rigid

330 predefined structure, a single mutation at the 11th LRRV position (**Fig. S1B**) to proline
331 significantly changes the conformation. Two of the Rbs (4J4L and 5B4P) have such proline
332 residues (at LRRV1 and LRRV2 respectively). These two Rbs were modeled using each other as
333 templates. One LRRV unit of the EGFR Rb (4UIP) was omitted. The trimmed Rb structure was
334 reconstructed by splitting the free Rb at LRRV3 and superimposing the LRRV3 on LRRV2 of the
335 complete Rb using PyMol.

336

337 **Preparation of Fc Variants**

338 The sequence of the human Fc binder repebody (RbF4) was obtained from a previously published
339 study [30]. The Rb structure was modeled using MODELLER with a free form (3RFS:A) as a
340 template structure. A free form of the hFc domain (3AVE) was used. Trastuzumab (trade name,
341 Herceptin) Fc sequence available from the literature (wild-type) and all subsequent variants were
342 reverse translated, codon optimized for expression in mammalian cells, and synthesized by
343 Integrated DNA technologies (IDT), Inc. (Redwood City, CA). CMVR VRC01 expression vector
344 (NIH AIDS reagent program, Germantown, MD) harboring the wild-type Fc or the Fc variant
345 sequences was transfected into suspension HEK 293 cells using polyethylenimine (PEI)
346 (Polysciences, Warrington, PA). Briefly, 500 µg of the wild-type Fc or Fc variant DNA was
347 combined with 1 ml of PEI and incubated at room temperature for 10 minutes. The mixture was
348 then added to HEK cells in the suspension and incubated in a humidified chamber at 37 °C with
349 8% CO_2 for at least 5 to 6 days. The secreted wild-type Fc or Fc variants were clarified through
350 centrifugation at 8000 rpm at 4 °C for 15 minutes on a Beckman Avanti-J25 centrifuge (Brea, CA).
351 The resulting supernatant was filtered through a 0.45 µm filter to remove any residual cell debris
352 and other large particles before loading onto a FPLC column.

353 Affinity purification was conducted on a pre-packed 5 ml Protein A column (for wild-type Fc, and
354 Fc variants 1 and 2) or pre-packed 5 ml Protein G column (for Fc variant 3, and single mutations
355 of the variant) from GE Healthcare (Pittsburgh, PA) as suggested by the manufacturer. The final
356 sample was eluted with 100 mM Glycine at pH 3 in 2 ml Eppendorf tubes prefilled with 50 µl of
357 1 M Tris and 5 mM EDTA. The purification process was automated on an AKTA FPLC system
358 (GE Healthcare, Pittsburgh, PA). The purified protein was subjected to a second buffer exchange
359 step using a hitrap desalting column (GE Healthcare, Pittsburgh, PA). The final product was eluted
360 in phosphate buffer saline and stored at -20 °C until further use. The purified proteins were
361 analyzed under reduced SDS-PAGE conditions and stained with coomassie blue.

362

363 **Expression and Purification of Repebodies**

364 The gene-encoding repebodies were inserted into NdeI and XhoI restriction sites of a pET21a
365 vector (Invitrogen, Carlsbad, CA). Plasmids were cloned into competent *E.coli* DH5α cells using
366 a heat shock method (at 42 °C for 90 seconds). The recombinant plasmids were transformed into
367 *E.coli* Origami-B cells (Merck, Kenilworth, NJ). Single colonies were inoculated into 5 mL of a
368 Luria-Bertani (LB) medium containing 50 µg/mL carbenicillin and grown overnight at 37 °C in a
369 shaking incubator (200 rpm). A total of 250 mL of LB containing 50 µg/mL carbenicillin was
370 inoculated with an OD_{600} 0.05 volume of the overnight-saturated culture and grown at 37 °C with
371 shaking at 200 rpm until the OD_{600} reached 0.5–0.8. The cells were induced using 0.5 mM IPTG
372 and incubated at 18 °C with shaking at 200 rpm for 16 hours. The cells were harvested through
373 centrifugation at 8000 rpm for 20 mins and suspended in a lysis buffer (50 mM NaH_2PO_4, 300 mM
374 NaCl, and 10 mM imidazole, at pH 8.0). After cell lysis by sonication, the cell debris was removed
375 through centrifugation at 16,000 rpm for 1 hour at 4 °C. Cell lysates were loaded into a Ni-NTA

376 column (Qiagen, Hilden, Germany) and washed using a wash buffer solution (50 mM NaH_2PO_4,
377 300 mM NaCl, 20 mM imidazole, at pH 8.0). The repebodies were eluted using an elution buffer
378 (50 mM NaH_2PO_4, 300 mM NaCl, 250 mM imidazole, at pH 8.0), and further purified using gel
379 permeation chromatography (Superdex 75, GE Healthcare). The buffer of the purified repebodies
380 changed into PBS, and the concentrate was developed in an AmiconUltra centrifugal filter (10 kDa
381 cutoff, Millipore).

382

383 **Determination of crystal structure**

384 The Fc domain of human IgG (hFc) was purified after digestion of the purchased human IgG
385 (Sigma, St. Louis, MO) with papain, as described elsewhere [47]. The RbF4-hFc complex was
386 purified through gel-filtration with a buffer containing 5 mM Tris·HCl and 0.1 M NaCl (pH 7.4)
387 after reconstitution of the complex by incubating RbF4 and hFc at a 2:1 molar ratio on ice. Crystals
388 of the complex were grown using a hanging drop vapor diffusion method against a crystallization
389 buffer containing 0.1 M sodium acetate, 12% (w/v) polyethylene glycol 6000, and 0.1 M
390 magnesium chloride (pH 4.6) at 20°C. The crystals formed in the space group $P2_12_12_1$ with a =
391 59.9 Å, b = 107.4 Å, and c = 171.4 Å, and contained one complex molecule in an asymmetric unit.
392 The diffraction data were collected at 100 K, with crystals flash-frozen in a crystallization buffer
393 containing 30% glycerol. A single-wavelength (1 Å) dataset was collected using a native crystal
394 on beam line 5C (Pohang Accelerator laboratory, Korea). Integration, scaling, and merging of the
395 diffraction data were conducted using the HKL2000 program suite [48]. The initial phases were
396 determined through molecular replacement using the Phenix AutoMR program [49] and human Fc
397 of IgG (PDB accession 1H3X) and repebody (PDB accession 3RFJ) as models. Successive rounds

398 of model building using Coot [50], refinement using the Phenix program [51], and phase
399 combination allowed the building of the complete structure (**Table S1**).

400

401 **Isothermal Titration Calorimetry (ITC)**

402 A binding affinity experiment was conducted using MicroCal-iTC200 (Malvern Instruments,
403 Malvern, UK). Fc variants, mouse IgG_1, and rabbit IgG (Sigma) were diluted in a PBS buffer to a
404 final concentration of 0.02 mM. RbF4 or RbF4-LT (RbF4 with the loop truncation) was diluted
405 using the same buffer to a final concentration of 0.2 mM. The ITC experiments were performed
406 for a total 20 injections and stirred at 1000 rpm. The initial injection of 1 μL was excluded for data
407 analysis. Titration curves were fitted with a one-site binding model. The value of K_d was
408 determined using Origin (OriginLab).

409

410 **Acknowledgements**

411 This work was supported by the Global Research Laboratory (NRF-2015K1A1A2033346) and
412 Mid-Career Researcher Program (NRF-2017R1A2A1A05001091) through the National Research
413 Foundation (NRF) of Korea, funded by the Ministry of Science and ICT. Y.C. was supported by
414 the Korea Research Fellowship Program (NRF-2016H1D3A1938246) through the National
415 Research Foundation of Korea, funded by the Ministry of Science and ICT. J.M. was supported
416 by Basic Science Research Program (NRF-2017R1A6A3A04012313) of the National Research
417 Foundation funded by the Ministry of Science and ICT, and the Ministry of Education. The
418 production of the Fc and Fc variant was supported by the National Institute of General Medical

Sciences of the U.S. National Institutes of Health under award numbers P20-GM113132 and 2R01GM098977.

Contributions

Y.C. designed the computational methods, and implemented and applied them to generate all of the computational results. S.J. conducted all in vitro experiments. J-M.C. determined the X-ray crystal structure. C.N. generated the Fc variants. Y.C., S.J., J-M.C., C.N., C.B-K., K.E.G., and H-S.K. designed and analyzed all of the prospective and retrospective tests and contributed toward the preparation of the manuscript.

Conflict of Interest: Chris Bailey-Kellogg and Karl E. Griswold are Dartmouth faculties and co-members of Stealth Biologics, LLC, a Delaware biotechnology company. These authors acknowledge that there may be a potential financial conflict of interest related to their associations with this company, and they hereby affirm that the data presented in this paper are free of any bias. This work has been reviewed and approved as specified in the conflict of interest management plans of Dartmouth.

References

1. Gan HK, Burgess AW, Clayton AH, Scott AM. Targeting of a conformationally exposed, tumor-specific epitope of EGFR as a strategy for cancer therapy. Cancer Res. 2012;72(12):2924-30.
2. Garrett TP, Burgess AW, Gan HK, Luwor RB, Cartwright G, Walker F, et al. Antibodies specifically targeting a locally misfolded region of tumor associated EGFR. Proc Natl Acad Sci USA. 2009;106(13):5082-7.
3. Khurana S, Fuentes S, Coyle EM, Ravichandran S, Davey Jr RT, Beigel JH. Human antibody repertoire after VSV-Ebola vaccination identifies novel targets and virus-neutralizing IgM antibodies. Nat Med. 2016;22(12):1439.
4. Kim KM, Shin EY, Moon JH, Heo TH, Lee JY, Chung Y, et al. Both the epitope specificity and isotype are important in the antitumor effect of monoclonal antibodies against Her-2/neu antigen. Int J Cancer. 2002;102(4):428-34.
5. Lewis GK. Challenges of antibody-mediated protection against HIV-1. Expert Rev Vaccines. 2010;9(7):683-7.
6. Zolla-Pazner S. Identifying epitopes of HIV-1 that induce protective antibodies. Nat Rev Immunol. 2004;4(3):199.
7. Abbott WM, Damschroder MM, Lowe DC. Current approaches to fine mapping of antigen–antibody interactions. Immunology. 2014;142(4):526-35.
8. Gao J, Kurgan L. Computational prediction of B cell epitopes from antigen sequences. Immunoinformatics: Springer; 2014. p. 197-215.
9. Zhang W, Xiong Y, Zhao M, Zou H, Ye X, Liu J. Prediction of conformational B-cell epitopes from 3D structures by random forests with a distance-based feature. BMC Bioinform. 2011;12(1):341.
10. Hogues H, Gaudreault F, Corbeil CR, Deprez C, Sulea T, Purisima EO. ProPOSE: Direct Exhaustive Protein–Protein Docking with Side Chain Flexibility. J Chem Theory Comput. 2018;14(9):4938-47.
11. Hua CK, Gacerez AT, Sentman CL, Ackerman ME, Choi Y, Bailey-Kellogg C. Computationally-driven identification of antibody epitopes. eLife. 2017;6:e29023.
12. Huang S-Y. Exploring the potential of global protein–protein docking: an overview and critical assessment of current programs for automatic ab initio docking. Drug Discov Today. 2015;20(8):969-77.
13. Sela-Culang I, Ofran Y, Peters B. Antibody specific epitope prediction—emergence of a new paradigm. Cur Opin Virol. 2015;11:98-102.
14. Houk K, Liu F. Holy grails for computational organic chemistry and biochemistry. Acc Chem Res. 2017;50(3):539-43.
15. Kastritis PL, Moal IH, Hwang H, Weng Z, Bates PA, Bonvin AM, et al. A structure-based benchmark for protein–protein binding affinity. Protein Sci. 2011;20(3):482-91.
16. Siebenmorgen T, Zacharias M. Computational prediction of protein–protein binding affinities. Wiley Interdiscip Rev Comput Mol Sci. 2020;10(3):e1448.
17. Sirin S, Apgar JR, Bennett EM, Keating AE. AB-Bind: antibody binding mutational database for computational affinity predictions. Protein Sci. 2016;25(2):393-409.
18. Lensink MF, Wodak SJ. Blind predictions of protein interfaces by docking calculations in CAPRI. Proteins. 2010;78(15):3085-95.
19. Grove TZ, Cortajarena AL, Regan L. Ligand binding by repeat proteins: natural and designed. Curr Opin Struct Biol. 2008;18(4):507-15.

481 20. Akira S, Takeda K, Kaisho T. Toll-like receptors: critical proteins linking innate and
482 acquired immunity. Nat Immunol. 2001;2(8):675.
483 21. Medzhitov R. Toll-like receptors and innate immunity. Nat Rev Immunol. 2001;1(2):135.
484 22. Pancer Z, Saha NR, Kasamatsu J, Suzuki T, Amemiya CT, Kasahara M, et al. Variable
485 lymphocyte receptors in hagfish. Proc Natl Acad Sci USA. 2005;102(26):9224-9.
486 23. Sutoh Y, Kasahara M. Lymphocyte Populations in Jawless Vertebrates: Insights Into the
487 Origin and Evolution of Adaptive Immunity. The Evolution of the Immune System: Elsevier;
488 2016. p. 51-67.
489 24. De Wit J, Hong W, Luo L, Ghosh A. Role of leucine-rich repeat proteins in the
490 development and function of neural circuits. Annu Rev Cell Dev Biol. 2011;27:697-729.
491 25. van der Biezen EA, Jones JD. The NB-ARC domain: a novel signalling motif shared by
492 plant resistance gene products and regulators of cell death in animals. Curr Biol. 1998;8(7):R226-
493 R8.
494 26. Deretic V, Saitoh T, Akira S. Autophagy in infection, inflammation and immunity. Nat
495 Rev Immunol. 2013;13(10):722.
496 27. Björklund ÅK, Ekman D, Elofsson A. Expansion of protein domain repeats. PLOS Comput
497 Biol. 2006;2(8):e114.
498 28. Enkhbayar P, Kamiya M, Osaki M, Matsumoto T, Matsushima N. Structural principles of
499 leucine-rich repeat (LRR) proteins. Proteins. 2004;54(3):394-403.
500 29. Lee S-C, Park K, Han J, Lee J-j, Kim HJ, Hong S, et al. Design of a binding scaffold based
501 on variable lymphocyte receptors of jawless vertebrates by module engineering. Proc Natl Acad
502 Sci USA. 2012;109(9):3299-304.
503 30. Heu W, Choi J-M, Lee J-J, Jeong S, Kim H-S. Protein binder for affinity purification of
504 human immunoglobulin antibodies. Anal Chem. 2014;86(12):6019-25.
505 31. Jeong S, Heu W, Kim J-w, Kim H-S. Protein binders specific for immunoglobulin g from
506 different species for immunoassays and multiplex imaging. Anal Chem. 2016;88(23):11938-45.
507 32. Kozakov D, Hall DR, Xia B, Porter KA, Padhorny D, Yueh C, et al. The ClusPro web
508 server for protein–protein docking. Nat Protoc. 2017;12(2):255.
509 33. Hornak V, Abel R, Okur A, Strockbine B, Roitberg A, Simmerling C. Comparison of
510 multiple Amber force fields and development of improved protein backbone parameters. Proteins.
511 2006;65(3):712-25.
512 34. Ponder JW. TINKER: Software tools for molecular design. Washington University School
513 of Medicine, Saint Louis, MO. 2004;3.
514 35. Schymkowitz J, Borg J, Stricher F, Nys R, Rousseau F, Serrano L. The FoldX web server:
515 an online force field. Nucleic Acids Res. 2005;33(suppl_2):W382-W8.
516 36. Choi Y, Furlon JM, Amos RB, Griswold KE, Bailey-Kellogg C. DisruPPI: structure-based
517 computational redesign algorithm for protein binding disruption. Bioinformatics.
518 2018;34(13):i245-i53.
519 37. Lee Jj, Choi HJ, Yun M, Kang Y, Jung JE, Ryu Y, et al. Enzymatic prenylation and oxime
520 ligation for the synthesis of stable and homogeneous protein–drug conjugates for targeted therapy.
521 Angew Chem Int Ed Engl. 2015;54(41):12020-4.
522 38. Hwang D-E, Choi J-M, Yang C-S, Lee J-j, Heu W, Jo E-K, et al. Effective suppression of
523 C5a-induced proinflammatory response using anti-human C5a repebody. Biochem Biophys Res
524 Commun. 2016;477(4):1072-7.
525 39. Chuang G-Y, Kozakov D, Brenke R, Comeau SR, Vajda S. DARS (Decoys As the
526 Reference State) potentials for protein-protein docking. Biophys J. 2008;95(9):4217-27.

527 40. Brenke R, Hall DR, Chuang G-Y, Comeau SR, Bohnuud T, Beglov D, et al. Application
528 of asymmetric statistical potentials to antibody–protein docking. Bioinformatics.
529 2012;28(20):2608-14.
530 41. De Vries SJ, Van Dijk M, Bonvin AM. The HADDOCK web server for data-driven
531 biomolecular docking. Nat Protoc. 2010;5(5):883.
532 42. Dominguez C, Boelens R, Bonvin AM. HADDOCK: a protein− protein docking approach
533 based on biochemical or biophysical information. J Am Chem Soc. 2003;125(7):1731-7.
534 43. Vajda S, Kozakov D. Convergence and combination of methods in protein–protein docking.
535 Curr Opin Struct Biol. 2009;19(2):164-70.
536 44. Rosenfeld L, Heyne M, Shifman JM, Papo N. Protein engineering by combined
537 computational and in vitro evolution approaches. Trends Biochem Sci. 2016;41(5):421-33.
538 45. Still WC, Tempczyk A, Hawley RC, Hendrickson T. Semianalytical treatment of solvation
539 for molecular mechanics and dynamics. J Am Chem Soc. 1990;112(16):6127-9.
540 46. Eswar N, Webb B, Marti-Renom MA, Madhusudhan M, Eramian D, Shen My, et al.
541 Comparative protein structure modeling using Modeller. Curr Protoc Bioinformatics.
542 2006;15(1):5.6. 1-5.6. 30.
543 47. Coleman L, Mahler SM. Purification of Fab fragments from a monoclonal antibody papain
544 digest by Gradiflow electrophoresis. Protein Expr Purif. 2003;32(2):246-51.
545 48. Otwinowski Z, Minor W. Processing of X-ray diffraction data collected in oscillation mode.
546 Meth Enzymol. 1997;276:307-26.
547 49. Adams PD, Afonine PV, Bunkóczi G, Chen VB, Davis IW, Echols N, et al. PHENIX: a
548 comprehensive Python-based system for macromolecular structure solution. Acta Crystallogr D.
549 2010;66(2):213-21.
550 50. Emsley P, Cowtan K. Coot: model-building tools for molecular graphics. Acta Crystallogr
551 D. 2004;60(12):2126-32.
552 51. Adams PD, Grosse-Kunstleve RW, Hung L-W, Ioerger TR, McCoy AJ, Moriarty NW, et
553 al. PHENIX: building new software for automated crystallographic structure determination. Acta
554 Crystallogr D. 2002;58(11):1948-54.

555

556

557 **Table 1. Test sets.** The numbers in parentheses indicate results from ClusPro without the antibody
558 mode option. For C5a, the numbers with asterisks (*) are results using the crystal structure for
559 docking with the precise definition of paratopes.

Target		**Human IgG Fc**	**Crystal Structure Complexes**		
			Interleukin 6 (IL-6)	Epidermal Growth Factor Receptor (EGFR)	Complement Component 5a (C5a)
Complex (PDB)		6KA7	4J4L	4UIP	5B4P
Rb homology template		3RFS	5B4P	3RFS	4J4L
Unbound target		3AVE	1ALU	1NQL	1KJS
Cα RMSD (Å)	Target	1.72	0.92	2.62	1.76
	Repebody	1.39	0.63	1.62	1.17
Number of docking models		29	30 (106)	30 (88)	23 (65) | ***28**
Number of EpiScope Designs		3	4	2	2
Number of localized docking models		7	5 (11)	12 (20)	6 (34) | ***7**
Best I-RMSD (Å)		2.32	1.45 (1.78)	2.23 (6.61)	3.61 (5.53) | ***0.62**
Best f_{nat}		0.43	0.62 (0.49)	0.38 (0.09)	0.27 (0.14) | ***0.76**

560

561

562 **Figure 1. Epitope localization and binding mode identification of human IgG_1 Fc (hFc)-**
563 **binding repebody (RbF4).** (**A**) EpiScope designs triple mutants considering the symmetry of the
564 Fc structure. (**B**) The set of the three mutations of Var 3 (H310A, N315K, and H435K) clearly
565 disrupts the binding, and the single mutations comprising Var 3 were individually test. The ITC
566 results indicate that H435K may not be involved in binding. Error bars represent variation over
567 ITC triplicates. Details are provided in **Fig. S2.** (**C**) There are seven docking models in contact
568 with H310A and N315K; the one colored blue had the lowest molecular modeling energy. (**D**)
569 Closer inspection of the model suggests that the repebody loop (highlighed in red stick; see also
570 **Fig. S1**) may be responsible for the binding specificity of RbF4 to hFc. IgG from three species are
571 considered (human; mouse, mFc; and rabbit, rFc). The residues that all three share in common are
572 colored cyan; those common to two are gray, and those unique to one species are black.

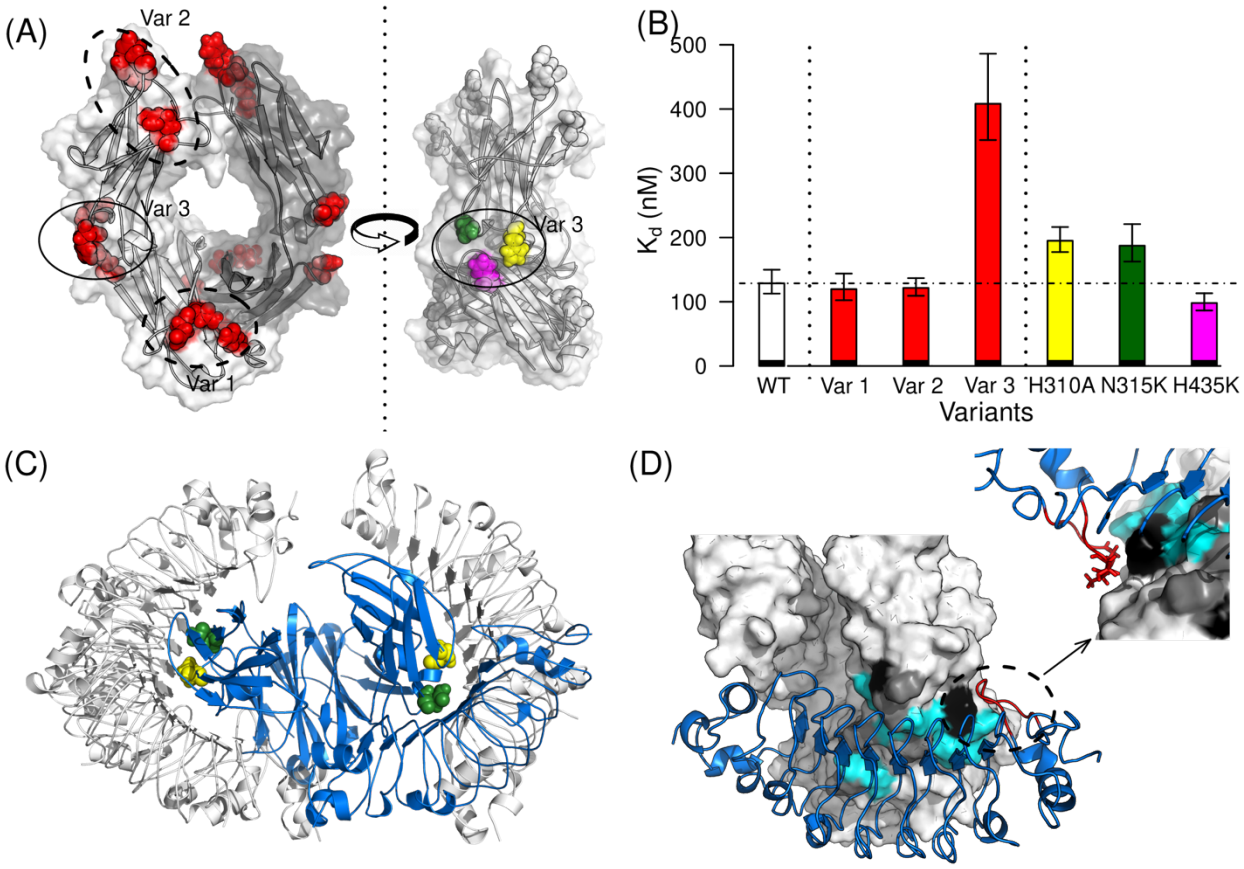

573

574

575 **Figure 2. Computationally-driven identification of the RbF4-hFc complex.** (**A**) The lowest-
576 energy model is in blue and the crystal structure (6KA7) is in gold. H310A and N315K are
577 highlighted in spheres (**B,C**) Comparison model energy vs. (**B**) I-RMSD and (**C**) f_{nat} Docking
578 models that are in contact with the epitope residues (correctly localized docking models) are shown
579 with solid circles. The crossed-circles are models in contact with all of the three residues in Var 3.
580 The blue circle is the model with the lowest force field energy (AMBER99sb) score (illustrated in
581 panel A).

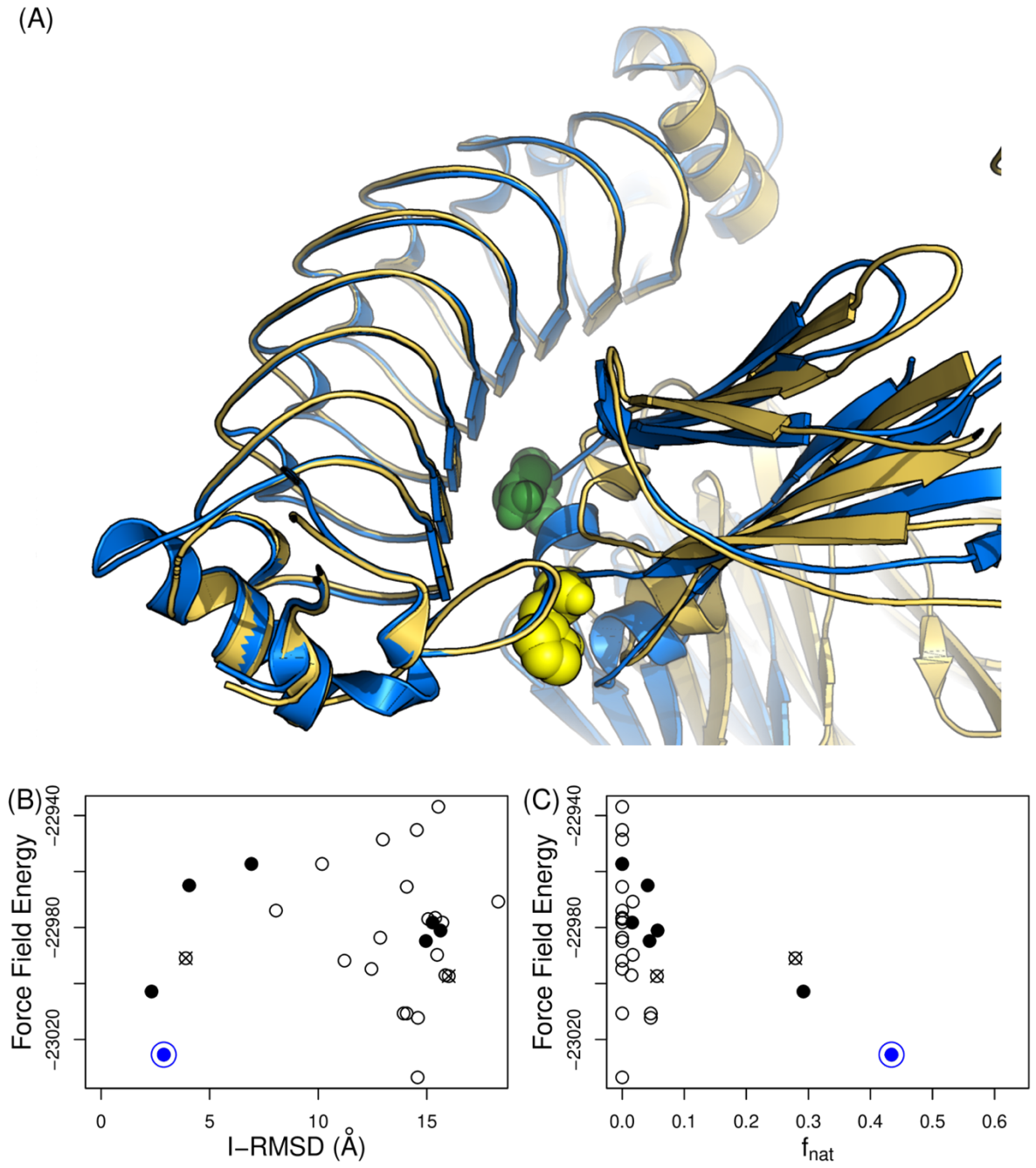

582

583 **Figure 3. Redesigning binding specificity and affinity based on modeled complex structure.**
584 The model suggests that the binding specificity of RbF4 comes from the loop (**Fig. 1D**). The loop
585 truncated RbF4 (RbF4-LT) was testing for binding against the IgGs from the three species. Further
586 computational design on the model identified mutations (S241M and S244R: RbF4-MR) that could
587 significantly improve the binding affinity for $mIgG_1$ (1 μM to 168.1 nM) while maintaining that
588 for $hIgG_1$ (**Table S3** for details). ITC-based affinity measurements were performed in triplate.

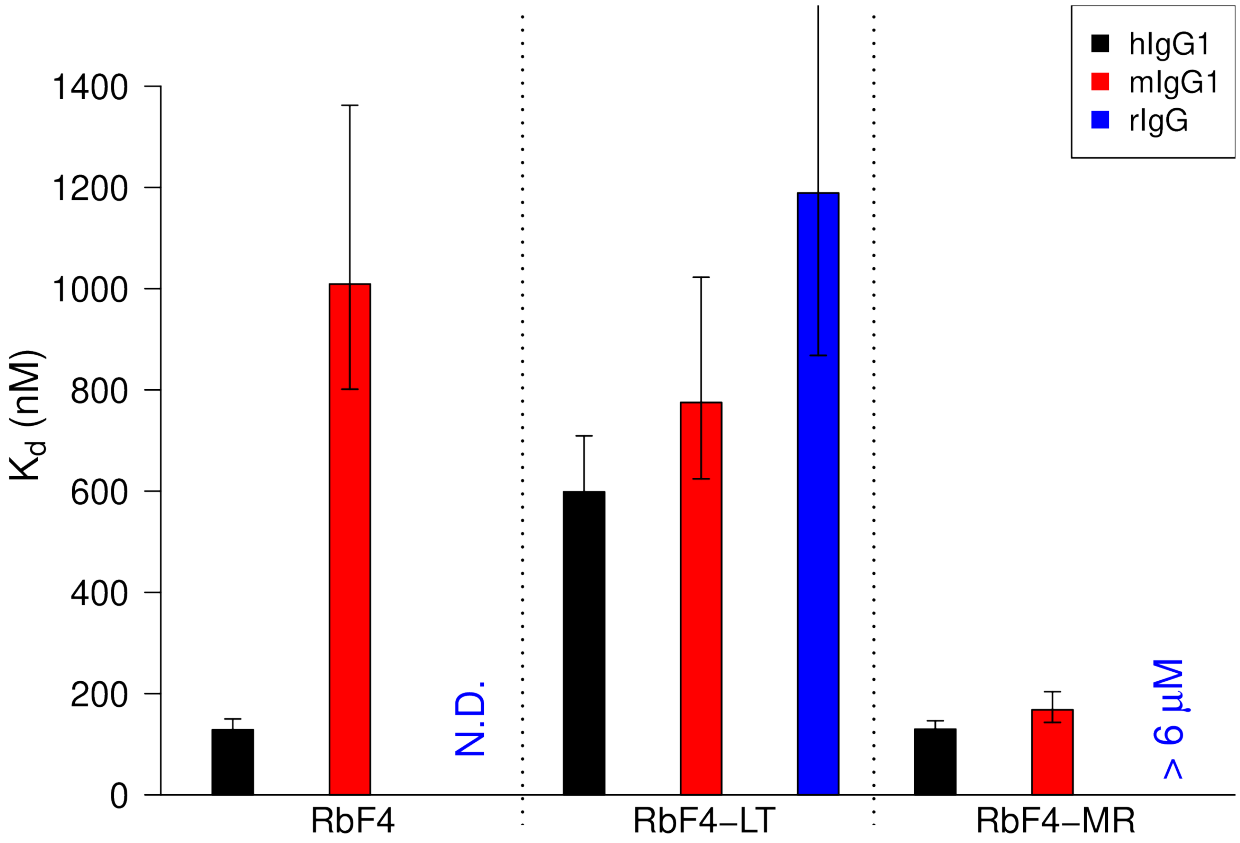

589
590

Figure 4. Retrospective tests of binding mode identification for additional targets. (**A**, **B, C**) IL-6; (**D**, **E**, **F**) EGFR; (**G**, **H**, **I**) C5a. (**A**, **D**, **G**) I-RMSD vs. energy; (**B**, **E**, **C**) f_{nat} vs. energy; (**C**, **F**, **I**) Points represent docking models, with those that are in contact with epitope residues (correctly localized docking models) shown as solid circles. The blue circle is the model with the minimum force field energy (AMBER99sb), and is native-like for IL-6 and EGFR. Wild-type (star) energy levels are depicted as dotted lines. For IL-6, some models have lower energy values than the most native-like docking model, indicating that ranking only by the force-field energy is not sufficient for binding mode prediction. (**C**, **F**, **I**) Crystal structures are in gold and the docking models with the lowest energies are in blue.

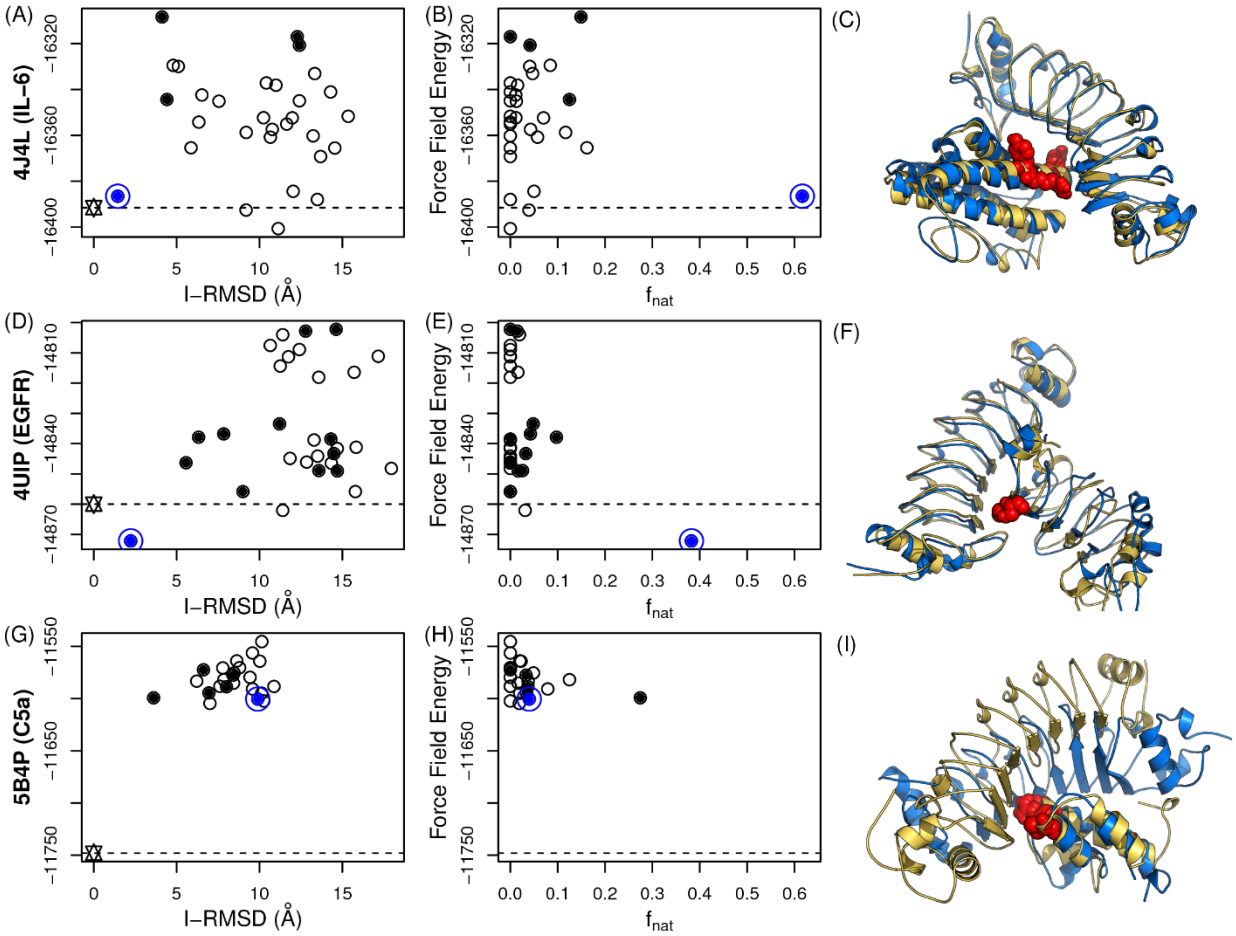

Figure 5. Impacts of high-quality structure and paratope definition. The incorporation of phage display results and the use of high quality structures (here crystal structures) lead to an extremely accurate identification of the binding mode. LRRV in blue is assigned for attraction, in red for repulsion and green for neutral (**A** and **H**). Results in the right two columns (**I-N**) are from docking models with precisely assigned paratopes. Docking models that are in contact with epitope residues (localized docking models) are in solid circle. Models with the minimum force field energy values are in blue circles. Wild-type (star) energy levels are depicted as dotted lines. Crystal structures are in gold and the docking models with the lowest energies are in blue.

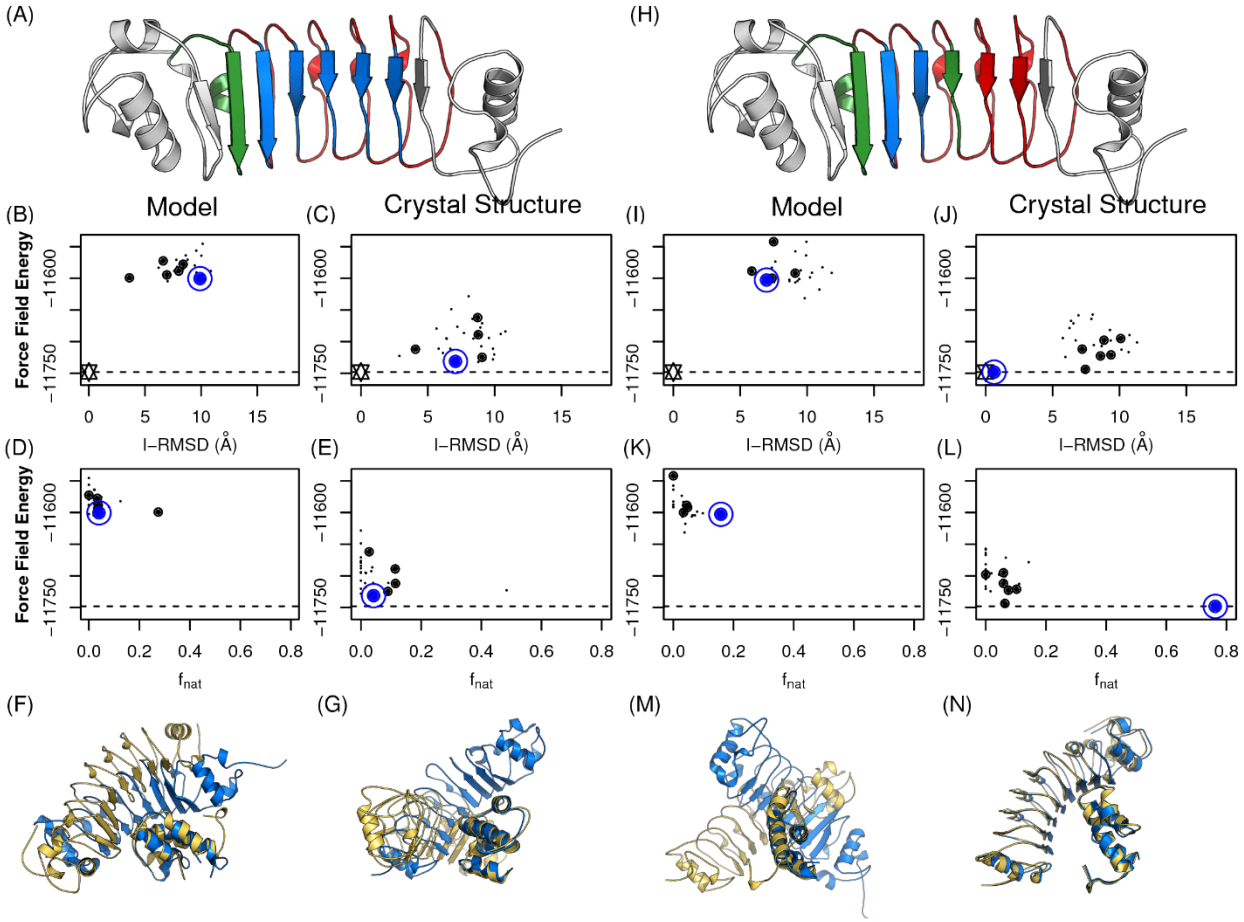

612 ## Supporting Information Captions

613

614 **Figure S1. The repebody structure.** (**A**) A repebody (Rb) largely consists of three parts: N-termianl cap
615 (LRRNT), variable regions (LRRV) and C-terminal cap (LRRCT). Binding occurs at the concave region
616 of LRRV (in darker blue). (**B**) Structure of a single LRRV motif, with side chains of conserved residues
617 rendered as stick figures. Each LRR is composed of six conserved leucine residues, a central conserved
618 asparagine residue, and conserved phenylalanine residue on the C-terminal side.

619

620 **Figure S2. Detailed information about the mutations for hFc-F4 epitope localization and titration**
621 **curves.** Based on the K_d values, H310 and N315 overlap epitopes.

622

623 **Figure S3. Docking models of RbF4.** The crystal structure is in gold. (A) The full atom energy
624 minimization step may change the overall structure, but the binding interactions are likely to be maintained.
625 The I-RMSD value of the lowest energy model (Model 1, blue) is slightly higher than the model with the
626 second lowest energy (Model 2, pink). However, its f_{nat} is twice higher. (B) There are two docking models
627 which are in contact with the three mutations in Var 3 (Model 9: cyan and Model 10: pink). While their
628 binding interface regions are largely correct, the binding orientation of the lower energy model (pink) is
629 completely inverted.

630

631 **Figure S4. Details of Binding affinities of RbF4 variants (RbF4, RbF4-LT and RbF4-MR) for $hIgG_1$,**
632 **$mIgG_1$ and rIgG.** RbF4 binds strongly to $hIgG_1$ and weakly to $mIgG_1$. However, no binding affinity is
633 measured for RbF4-rIgG. The truncation of the loop (RbF4-LT) enabled the variant to bind to all IgGs with
634 similar binding affinities. RbF4-MR gains strong binding affinities for $hIgG_1$ and $mIgG_1$. See
635 **Supplementary Table 2 3** for details.

636

637 **Figure S5. FoldX scan of the RbF4 loop.** The residue scan using FoldX suggests that the inclusion of the
638 loop may not enhance the binding affinity of RbF4 for rIgG.

639

640 **Figure S6. Predicted ΔΔG values of the RbF4 variants.** The variant with S241M and S244R mutations
641 (RbF4-MR) is predicted to strongly bind to both $hIgG_1$ and $mIgG_1$. S244C and S244P were not considered.

642

643 **Figure S7. Binding mode prediction with the ClusPro score.** Docking models that are in contact with
644 epitope overlapping residues (localized docking models) are in solid circle. The blue circle is the model
645 with the lowest ClusPro score. Crystal structures are in yellow and the docking models with the lowest
646 energies are in blue on the right hand side. Score assessment using the ClusPro score is not predictive.

647

648 **Table S1. Data collection and refinement statistics**

649

650 **Table S2. Quality measures and contact information of RbF4 docking models.** Each black block
651 indicates that the Fc position is in contact with the docked repebody.

652

653 **Table S3. *In silico* binding specificity control and affinity improvements.** RbF4 strongly binds to $hIgG_1$
654 (weakly to $mIgG_1$), but no binding to rIgG is observed. Removal of the loop (RbF4-LT) causes a slight
655 reduction in the binding affinity toward $hIgG_1$, but yields a marginal affinity improvement for $mIgG_1$.
656 RbF4-LT produces a significant improvement in the affinity for rIgG. RbF4 with two mutations at 241 and
657 244 (S241M with S244R, RbF4-MR) binds to both $hIgG_1$ and $mIgG_1$ with high binding affinities.